Mixing rules for the piezoelectric properties of Macro Fiber Composites (MFC)

A. Deraemaeker[*], H. Nasser[+], A. Benjeddou [†] and A. Preumont[*]

[*] Active Structures Laboratory, ULB, 50 av. Franklin Roosevelt, CP 165/42, 1050 Brussels, Belgium
[+] CRP Henri Tudor, 29 Avenue John F. Kennedy, L-1855 Luxembourg
[†] Supméca Paris - LISMMA, 3 Rue Fernand Hainault, 93407 Saint Ouen CEDEX, France

Abstract

This paper focuses on the modelling of structures equipped with Macro Fiber Composite (MFC) transducers. Based on the uniform field method under the plane stress assumption, we derive analytical mixing rules in order to evaluate equivalent properties for d_{31} and d_{33} MFC transducers. In particular, mixing rules are derived for the longitudinal and transverse piezoelectric coefficients of MFCs. These mixing rules are validated using finite element computations and experimental results available from the literature.

1 Introduction

Piezoelectric actuators and sensors have been widely used in active vibration control applications. PZT ceramics are commonly used due to their good actuation capability and very wide bandwidth. The major drawbacks of these ceramics are their brittle nature, and the fact that they cannot be easily attached to curved structures. In order to overcome these drawbacks, two techniques have been developed : (i) thick film deposition of PZT [1] which requires that the part be heated at 900 ℃ for sintering, and (ii) using packaged PZT composites which can be glued on curved structures. This paper focuses on the second alternative.

A typical piezocomposite transducer is made of an active layer sandwiched between two soft thin encapsulating layers. The packaging plays two different roles : (i) applying prestress to the active layer in order to avoid cracks, and (ii) bringing the electric field to the active layer through the use of a specific surface electrode pattern. The first piezocomposite was developed at MIT [2]. It consisted of an active layer made of round PZT fibers surrounded by an epoxy matrix, actuated in the d_{31} mode (Figure 1a). A major problem with this kind of configuration comes from the very large difference in the dielectric permittivities of the piezoelectric fiber (ε_r=1850) and the epoxy matrix (ε_r=4). This results in a drastic reduction of the electric field applied to the active fiber, even for a very small layer of epoxy trapped between the electrodes and the fibers.

1

At the same period, Hagood also introduced the concept of interdigitated electrodes (Figure 1b) in order to drive the piezo transducers in the d_{33}-mode [3, 4]. The actuator performance is enhanced due to the higher value of the d_{33} coefficient, which is usually 2 to 3 times higher than the d_{31}. On the other hand, high voltages need to be used, because of the spacing of the finger electrodes which is 3 to 6 times higher than the thickness of the transducer.

Around the year 2000, the so-called MFCs (Macro Fiber Composites) have been developed at NASA [5]. The main difference with the previous attempts is that the fibers are rectangular, and diced from a regular ceramic. The manufacturing process is quite cheap and repeatable, and the shape of the fibers together with the manufacturing process allows to put the fibers in direct contact with the electrodes, therefore solving the problem of the permittivity mismatch. Both d_{31} and d_{33} transducers have been developed and are currently produced by the company *Smart Material* (Dresden, Germany). Our study focuses on MFC transducers.
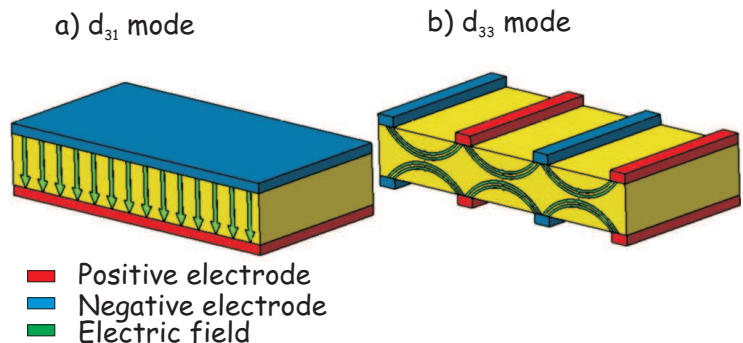

Figure 1: Electric field distribution for different electrode configurations

It is clear that many efforts have been spent to develop robust and efficient piezoelectric flat transducers [6, 7]. The modeling of such transducers attached to thin structures is however not straightforward. The analysis of multi-layer shells including piezoelectric layers can be performed using finite element formulations [8, 9]. Piezoelectric patches working in the d_{31} mode can be modelled by a single layer of PZT material. Piezocomposite transducers are made of several layers (electrode layer, glue layer, active layer), some of which may consist of different materials. For an accurate modelling of these devices, a detailed description of the layer sequence and thicknesses, as well as equivalent, homogeneous mechanical, piezoelectric and dielectric properties of each layer is needed. Most manufacturers only provide global information about the transducers, such as the total thickness, the free strain in the fiber direction, the blocking force, the capacitance, etc. This information is not sufficient to build accurate numerical models of structures with embedded piezocomposites.

The first attempts to model flat piezocomposites were conducted for AFCs [10, 4, 11]. Several methods were used in order to compute the equivalent properties of these devices : the uniform field method (UFM) which is a generalization of the series and parallel mixing rules first developed in [12] for piezocomposites, the self consistent approach [13], and finite element modelling [4]. For d_{33} MFCs, equivalent thermal expansion coefficients [14] and mechanical properties [15] have been derived analytically using classical mixing rules or slightly modified versions of them. Experiments have also been conducted in [16, 17] in order to identify the me-

chanical properties which were found to be in good agreement with the analytical predictions.

From the above literature review, it is thought that there exists no analytical simple mixing rules for the evaluation of the longitudinal and transverse piezoelectric coefficients for piezocomposites with rectangular fibers such as d_{31} and d_{33}-MFCs. As demonstrated in a previous study [18, 19], both the longitudinal and the transverse piezoelectric coefficients are important for a correct prediction of the performances of structures equipped with MFC transducers. This study aims at filling this gap by deriving simple analytical mixing rules for the piezoelectric coefficients of MFCs. The mixing rules are validated by finite element computations as well as comparison with experimental results available from the literature.

2 Constitutive equations of piezocomposite transducers

2.1 d_{31} - piezocomposites

For d_{31} piezocomposites, the poling direction (conventionally direction 3) is normal to the plane of the patches (Figure 2a) and according to the plane stress assumption $T_3 = 0$. The electric field is assumed to be aligned with the polarization vector ($E_2 = E_1 = 0$). Using the standard IEEE notations for linear piezoelectricity, and the Mindlin hypothesis, the constitutive equations are :

$$
\left\{ \begin{array}{c} S_1 \\ S_2 \\ S_4 \\ S_5 \\ S_6 \\ \hline D_3 \end{array} \right\} = \left[\begin{array}{ccccc|c} s_{11}^E & s_{12}^E & 0 & 0 & 0 & d_{31} \\ s_{21}^E & s_{22}^E & 0 & 0 & 0 & d_{32} \\ 0 & 0 & s_{44}^E & 0 & 0 & 0 \\ 0 & 0 & 0 & s_{55}^E & 0 & 0 \\ 0 & 0 & 0 & 0 & s_{66}^E & 0 \\ \hline d_{31} & d_{32} & 0 & 0 & 0 & \varepsilon_{33}^T \end{array} \right] \left\{ \begin{array}{c} T_1 \\ T_2 \\ T_4 \\ T_5 \\ T_6 \\ \hline E_3 \end{array} \right\} \tag{1}
$$

where E_i and D_i are the components of the electric field vector and the electric displacement vector, and T_i and S_i are the components of stress and strain vectors, defined according to :

$$
\left\{ \begin{array}{c} T_1 \\ T_2 \\ T_3 \\ T_4 \\ T_5 \\ T_6 \end{array} \right\} = \left\{ \begin{array}{c} T_{11} \\ T_{22} \\ T_{33} \\ T_{23} \\ T_{13} \\ T_{12} \end{array} \right\} \qquad \left\{ \begin{array}{c} S_1 \\ S_2 \\ S_3 \\ S_4 \\ S_5 \\ S_6 \end{array} \right\} = \left\{ \begin{array}{c} S_{11} \\ S_{22} \\ S_{33} \\ 2\,S_{23} \\ 2\,S_{13} \\ 2\,S_{12} \end{array} \right\} \tag{2}
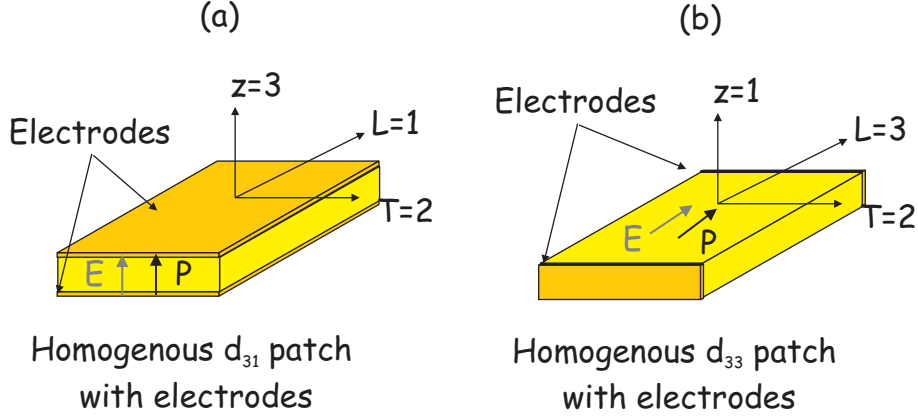$$

3

Figure 2: Homogeneous models of the piezoelectric layers with electrodes : reference frames for d_{31} and d_{33} piezoelectric layers

2.2 d_{33} - piezocomposites

For d_{33} piezocomposites, although the electric field lines do not have a constant direction (Figure 1b), it is reasonable to consider that the poling direction is that of the fibers (direction 3, Figure 2b), and that the electric field is in the same direction. With this reference frame, the plane stress hypothesis implies that $T_1 = 0$. The constitutive equations are given by

$$
\left\{
\begin{array}{c}
S_2 \\
S_3 \\
S_4 \\
S_5 \\
S_6 \\
\hline
D_3
\end{array}
\right\}
=
\left[
\begin{array}{ccccc|c}
s_{22}^E & s_{23}^E & 0 & 0 & 0 & d_{32} \\
s_{32}^E & s_{33}^E & 0 & 0 & 0 & d_{33} \\
0 & 0 & s_{44}^E & 0 & 0 & 0 \\
0 & 0 & 0 & s_{55}^E & 0 & 0 \\
0 & 0 & 0 & 0 & s_{66}^E & 0 \\
\hline
d_{32} & d_{33} & 0 & 0 & 0 & \varepsilon_{33}^T
\end{array}
\right]
\left\{
\begin{array}{c}
T_2 \\
T_3 \\
T_4 \\
T_5 \\
T_6 \\
\hline
E_3
\end{array}
\right\}
\tag{3}
$$

3 Mixing rules for MFC transducers

3.1 d_{31} MFCs

We consider a representative volume element (RVE, Figure 3) on which the average values of T_i, S_i, D_i, E_i are given by :

$$
\overline{T_i} = \frac{1}{V} \int_V T_i dV \qquad \overline{D_i} = \frac{1}{V} \int_V D_i dV \tag{4}
$$

$$
\overline{S_i} = \frac{1}{V} \int_V S_i dV \qquad \overline{E_i} = \frac{1}{V} \int_V E_i dV \tag{5}
$$

where $^-$ denotes the average value. Using the *uniform field method* (UFM, [20]), we assume that all the fields are uniform in each constituent. In addition, the deformation mechanisms used in the classical laminate theory and represented on Figure 4 are considered, leading to the following equalities :
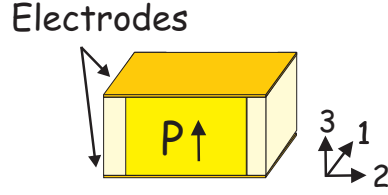
4

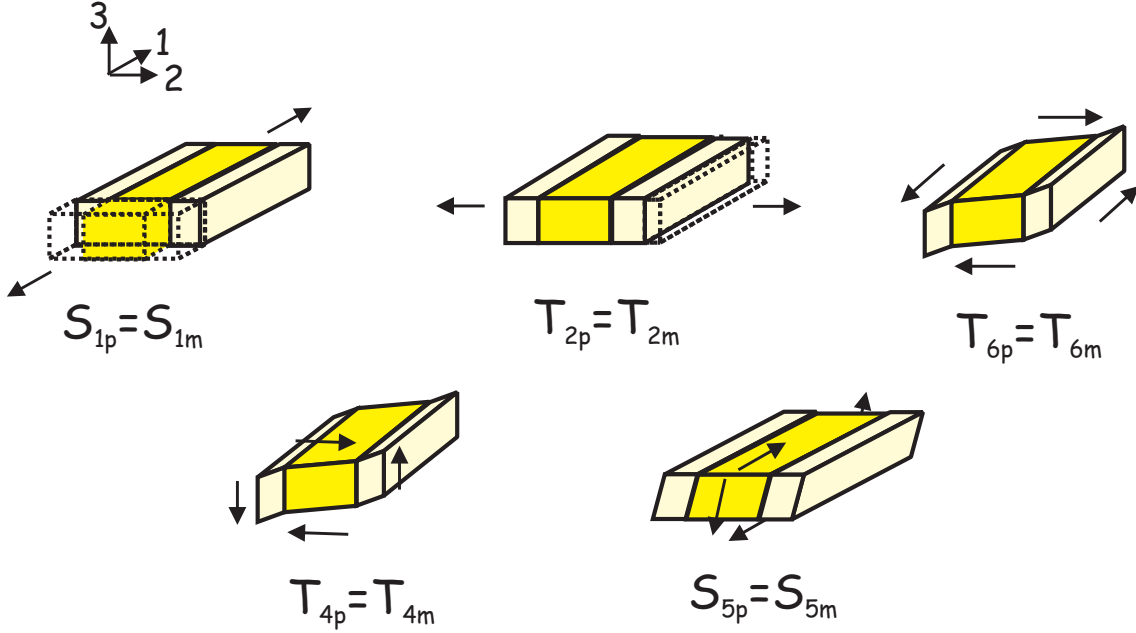Figure 3: Representative volume element (RVE) for a d_{31} MFC

Figure 4: Deformation mechanism for the RVE of a d_{31} MFC

$$\begin{aligned}
\overline{S_1} &= S_1^p &= S_1^m \\
\overline{T_2} &= T_2^p &= T_2^m \\
\overline{T_4} &= T_4^p &= T_4^m \\
\overline{S_5} &= S_5^p &= S_5^m \\
\overline{T_6} &= T_6^p &= T_6^m
\end{aligned} \tag{6}$$

where ^{p} denotes the piezoelectric material and ^{m} the matrix. For the other fields, the average values are given by :

$$\begin{aligned}
\overline{T_1} &= \rho T_1^p &+ (1-\rho)T_1^m \\
\overline{S_2} &= \rho S_2^p &+ (1-\rho)S_2^m \\
\overline{S_4} &= \rho S_4^p &+ (1-\rho)S_4^m \\
\overline{T_5} &= \rho T_5^p &+ (1-\rho)T_5^m \\
\overline{S_6} &= \rho S_6^p &+ (1-\rho)S_6^m
\end{aligned} \tag{7}$$

where ρ is the fiber volume fraction. Since the electrodes are continuous on the top and bottom of the RVE, the electrical potential difference (and therefore the electric field) is equal in the two phases :

$$\overline{E_3} \;=\; E_3^p \;=\; E_3^m;\tag{8}$$

and

$$\overline{D_3} \;=\; \rho D_3^p \;+\; (1-\rho)D_3^m,\tag{9}$$

Upon using the variables which are identical in the two phases as independent variables, the constitutive equations (1) are written in the form

$$\left\{\begin{array}{c} T_1 \\ S_2 \\ S_4 \\ T_5 \\ S_6 \\ D_3 \end{array}\right\} = A \left\{\begin{array}{c} S_1 \\ T_2 \\ T_4 \\ S_5 \\ T_6 \\ E_3 \end{array}\right\}\tag{10}$$

with

$$A = \begin{bmatrix} \frac{1}{s_{11}^E} & -\frac{s_{21}^E}{s_{11}^E} & 0 & 0 & 0 & -\frac{d_{31}}{s_{11}^E} \\ \frac{s_{21}^E}{s_{11}^E} & s_{22}^E - \frac{(s_{21}^E)^2}{s_{11}^E} & 0 & 0 & 0 & d_{32} - d_{31}\frac{s_{21}^E}{s_{11}^E} \\ 0 & 0 & s_{44}^E & 0 & 0 & 0 \\ 0 & 0 & 0 & \frac{1}{s_{55}^E} & 0 & 0 \\ 0 & 0 & 0 & 0 & s_{66}^E & 0 \\ \frac{d_{31}}{s_{11}^E} & d_{32} - d_{31}\frac{s_{21}^E}{s_{11}^E} & 0 & 0 & 0 & \epsilon_{33}^T - \frac{d_{31}^2}{s_{11}^E} \end{bmatrix}\tag{11}$$

Following (7), we have

$$\left\{\begin{array}{c} \overline{T_1} \\ \overline{S_2} \\ \overline{S_4} \\ \overline{T_5} \\ \overline{S_6} \\ \overline{D_3} \end{array}\right\} = \rho \left\{\begin{array}{c} T_1^p \\ S_2^p \\ S_4^p \\ T_5^p \\ S_6^p \\ D_3^p \end{array}\right\} + (1-\rho) \left\{\begin{array}{c} T_1^m \\ S_2^m \\ S_4^m \\ T_5^m \\ S_6^m \\ D_3^m \end{array}\right\}\tag{12}$$

Using (10), we get

$$\overline{A} \left\{\begin{array}{c} \overline{S_1} \\ \overline{T_2} \\ \overline{T_4} \\ \overline{S_5} \\ \overline{T_6} \\ \overline{E_3} \end{array}\right\} = \rho A_p \left\{\begin{array}{c} S_1^p \\ T_2^p \\ T_4^p \\ S_5^p \\ T_6^p \\ E_3^p \end{array}\right\} + (1-\rho) A_m \left\{\begin{array}{c} S_1^m \\ T_2^m \\ T_4^m \\ S_5^m \\ T_6^m \\ E_3^m \end{array}\right\}\tag{13}$$

and finally using equalities (6) and (8), we have:

$$\overline{A} = \rho A_p + (1-\rho)A_m\tag{14}$$

Each term of matrix A follows therefore a linear mixing rule. Rearranging those linear relationships and writing them in terms of engineering constants, we get :

6

$$E_L = \rho\, E_L^p + (1 - \rho)\, E_L^m \tag{15}$$

$$\frac{1}{E_T} = \frac{\rho}{E_T^p} + \frac{1 - \rho}{E_T^m} \tag{16}$$

$$\nu_{LT} = \rho\, \nu_{LT}^p + (1 - \rho)\, \nu_{LT}^m \tag{17}$$

$$\frac{1}{G_{LT}} = \frac{\rho}{G_{LT}^p} + \frac{1 - \rho}{G_{LT}^m} \tag{18}$$

$$G_{Lz} = \rho\, G_{Lz}^p + (1 - \rho)\, G_{Lz}^m \tag{19}$$

$$\frac{1}{G_{Tz}} = \frac{\rho}{G_{Tz}^p} + \frac{1 - \rho}{G_{Tz}^m} \tag{20}$$

where E_L denotes the longitudinal Young's modulus (in the fibre direction), E_T the transverse modulus, ν_{LT} is the major Poisson's ratio, G_{LT} is the in-plane shear modulus and G_{Tz}, G_{Lz} are the two out-of-plane shear moduli. For these mechanical properties, we obtain the classical mixing rules for layered composite materials [21] (note that some minor terms have been neglected in the expression of E_T). For the piezoelectric and dielectric properties, we find :

$$d_{31} = \frac{1}{E_L}\rho\, d_{31}^p\, E_L^p \tag{21}$$

$$d_{32} = -d_{31}\, \nu_{LT} + \rho\, d_{31}^p\, (1 + \nu_{LT}^p) \tag{22}$$

$$\epsilon_{33}^T = \rho\epsilon_{33}^{Tp} + (1 - \rho)\epsilon_{33}^{Tm} \tag{23}$$

where we have considered that the matrix is not piezoelectric and that $d_{31} = d_{32}$ for the fibers. It is interesting to note that **these expressions are identical to the mixing rules for thermal expansion coefficients** [21, 22] (d_{31} needs to be replaced by the thermal expansion coefficient α for the analogy). d_{31} follows a linear mixing rules involving only longitudinal properties (E_L^p, E_L^m and d_{31}^p), whereas d_{32} depends on longitudinal as well as transverse properties. For the permittivity, the relationship correspond to the parallel rule for capacitors (here also, some minor terms due to the piezoelectric coupling have been neglected).

3.2 d_{33} MFCs

Figure 5 shows the RVE for a d_{33} MFC. Using the *uniform field method*, we assume that all the fields are uniform in each constituent. In addition, deformation mechanisms identical to the ones considered for the d_{31} MFCs (Figure 4) are considered, leading to the following equalities :
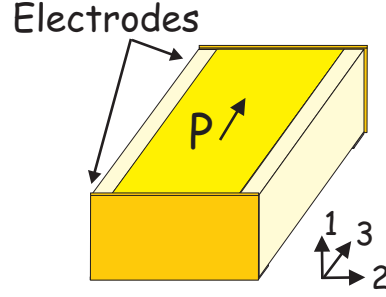
Figure 5: Representative volume element (RVE) for a d_{33} MFC

$$\begin{aligned}
\overline{S_3} &= S_3^p = S_3^m \\
\overline{T_2} &= T_2^p = T_2^m \\
\overline{T_4} &= T_4^p = T_4^m \\
\overline{S_5} &= S_5^p = S_5^m \\
\overline{T_6} &= T_6^p = T_6^m
\end{aligned} \qquad (24)$$

For the other fields, the average values are given by :

$$\begin{aligned}
\overline{T_3} &= \rho T_3^p + (1-\rho)T_3^m \\
\overline{S_2} &= \rho S_2^p + (1-\rho)S_2^m \\
\overline{S_4} &= \rho S_4^p + (1-\rho)S_4^m \\
\overline{T_5} &= \rho T_5^p + (1-\rho)T_5^m \\
\overline{S_6} &= \rho S_6^p + (1-\rho)S_6^m
\end{aligned} \qquad (25)$$

Since the electrodes are continuous on the front and rear of the RVE, the electrical potential difference (and therefore the electric field) is equal in the two phases :

$$\overline{E_3} = E_3^p = E_3^m; \qquad (26)$$

and

$$\overline{D_3} = \rho D_3^p + (1-\rho)D_3^m, \qquad (27)$$

Following similar developments as before, we obtain the mixing rules which are summarized in Table 1 (assuming that the matrix is not piezoelectric and that $d_{31} = d_{32}$ for the fibers), and compared to the mixing rules developed for d_{31} MFCs.
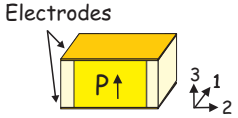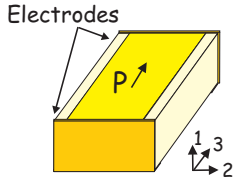
8

d_{31} **MFC**	d_{33} **MFC**
Electrodes	Electrodes

Mechanical Properties

$$E_L = \rho\, E_L^p + (1 - \rho)\, E_L^m$$
$$\frac{1}{E_T} = \frac{\rho}{E_T^p} + \frac{1 - \rho}{E_T^m}$$
$$\nu_{LT} = \rho\, \nu_{LT}^p + (1 - \rho)\, \nu_{LT}^m$$
$$\frac{1}{G_{LT}} = \frac{\rho}{G_{LT}^p} + \frac{1 - \rho}{G_{LT}^m}$$
$$G_{Lz} = \rho\, G_{Lz}^p + (1 - \rho)\, G_{Lz}^m$$
$$\frac{1}{G_{Tz}} = \frac{\rho}{G_{Tz}^p} + \frac{1 - \rho}{G_{Tz}^m}$$

Piezoelectric Properties

$d_{31} = \dfrac{1}{E_L} \rho\, d_{31}^p\, E_L^p$ $d_{32} = -d_{31}\, \nu_{LT} + \rho d_{31}^p \left(1 + \nu_{LT}^p\right)$	$d_{33} = \dfrac{1}{E_L} \left(\rho\, d_{33}^p\, E_L^p\right)$ $d_{32} = -d_{33}\, \nu_{LT} + \rho \left(d_{32}^p + d_{33}^p\, \nu_{LT}^p\right)$

Dielectric Properties

$$\epsilon_{33}^T = \rho\epsilon_{33}^{Tp} + (1 - \rho)\epsilon_{33}^{Tm}$$

Table 1: Summary of mixing rules for d_{31} and d_{33} MFCs

4 Numerical validation of the mixing rules for MFCs

In order to validate the mixing rules presented in the previous section, the homogenized properties of both d_{31} and d_{33} MFCs have been computed numerically using the finite element method. In total, six local problems are needed to identify all the coefficients of the piezoelectric constitutive equations. These are presented in Figure 6 for a d_{33}-MFC . The first problem consists in applying a voltage V to the electrodes of the RVE and imposing zero displacement on all the faces of the RVE, except the top and bottom (in order to model the plane stress condition). In the next five local problems, the difference of potential is set to 0 (short-circuited condition), and five deformation mechanisms are induced. Each of the deformation mechanisms consists in a unitary strain in one of the directions (with zero strain in

all the other directions). For each problem, the solution is computed using piezoelectric solid finite elements in SAMCEF [23]. The average values of T_i, S_i, D_i and E_i are computed and used to determine all the coefficients in the constitutive equations, from which the engineering constants are computed.

Note that in the finite element computations, the finger electrodes are modelled, resulting in a curved electric field when a voltage difference is applied across the electrodes. The poling of the PZT material is aligned with these curved electric field lines. This is in fact rarely done in such computations as it involves a complicated definition of the PZT properties which vary in the RVE. For these computations, the spacing between the interdigitated electrodes is five times the thickness of the transducer (typical value used in the early developments of MFCs).
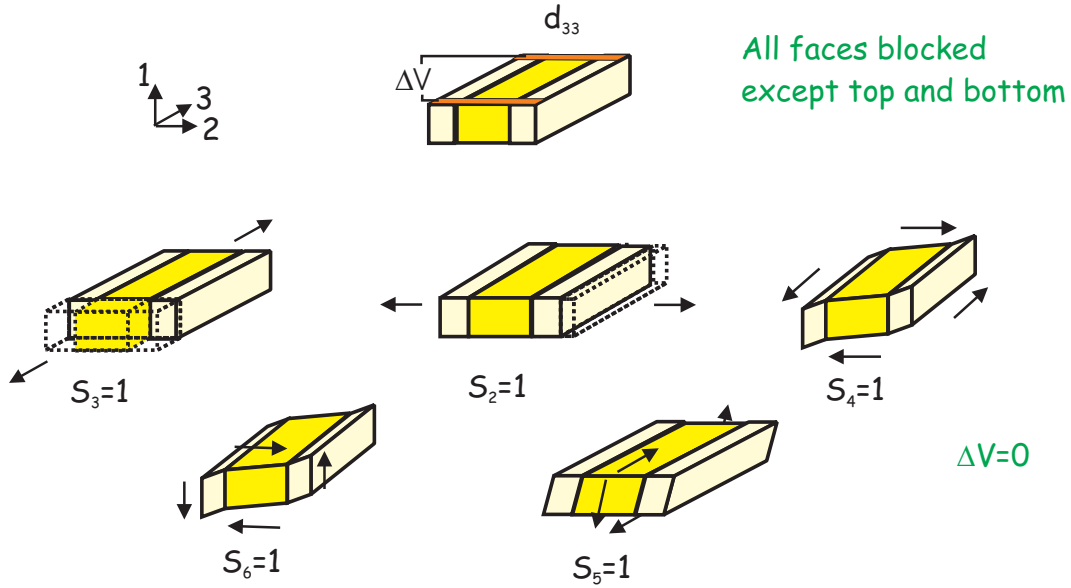

Figure 6: The six local problems solved by the finite element method in order to compute the homogenized properties of d_{33}-MFCs

The homogeneous properties of the active layer have been computed numerically for different values of the volume fraction of fibers ρ. These numerical results are compared with the analytical mixing rules developed in section 3. The properties of the fibers are given in Table 2 (it is assumed that the fibers are made of SONOX P502 from $CeramTec$, for more details, see [19]). For the matrix, typical isotropic values for epoxy are considered : $1/s_{11}^E = 1/s_{22}^E = 1/s_{33}^E = 2.9\ GPa$ (Young's modulus), $\nu = 0.3$ and $\varepsilon_{11}^T/\varepsilon_0 = \varepsilon_{22}^T/\varepsilon_0 = \varepsilon_{33}^T/\varepsilon_0 = 4.25$.

MFC Fiber Engineering constants	Symbol	Unit	SONOX P502
Young's modulus	$1/s_{11}^E = 1/s_{22}^E$	GPa	54.05
	$1/s_{33}^E$	GPa	48.30
Shear modulus	$2/s_{32}^E = 2/s_{31}^E$	GPa	19.48
	$2/s_{12}^E$	GPa	19.14
Poisson's ratio	$\nu_{23} = \nu_{13}$	-	0.44
	ν_{12}	-	0.41
Piezoelectric charge constants	$d_{32} = d_{31}$	pC/N	-185
	d_{33}	pC/N	440
	$d_{15} = d_{24}$	pC/N	560
Dieletric relative constants (free)	$\varepsilon_{11}^T/\varepsilon_0 = \varepsilon_{22}^T/\varepsilon_0$	-	1950
	$\varepsilon_{33}^T/\varepsilon_0$	-	1850

Table 2: MFC fibers engineering constants

The evolution of the piezoelectric properties as a function of the fiber volume fraction for d_{31}-MFCs is represented on Figure 7. The match between the analytical and the numerial results is very good for d_{31} and good for d_{32}.
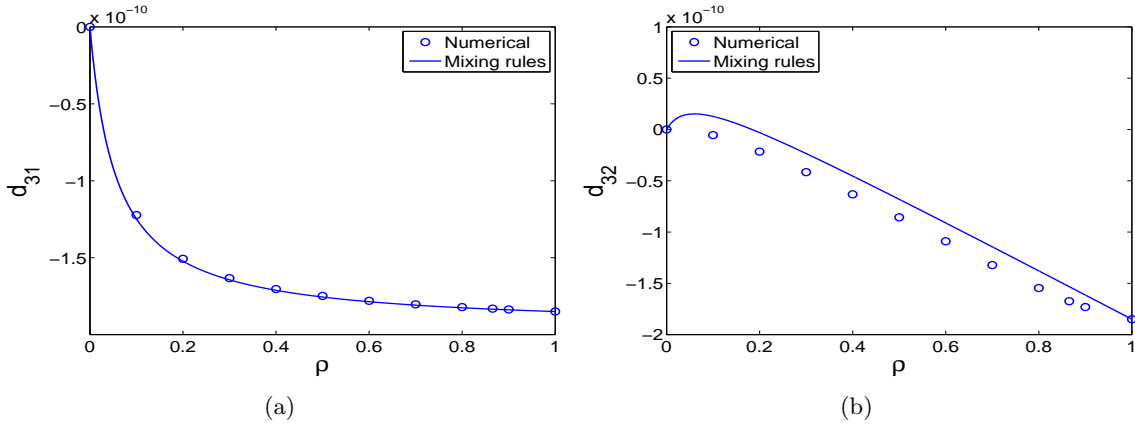

(a)   (b)

Figure 7: Evolution of piezoelectric properties of d_{31} MFCs as a function of the fiber volume fraction : comparison between the mixing rules and the finite element computations

The evolution of the piezoelectric properties of d_{33}-MFCs as a function of the fiber volume fraction is represented on Figure 8 and compared to the analytical mixing rules. The numerical values for d_{33} are slightly lower than the analytical ones, but the difference is not very large.
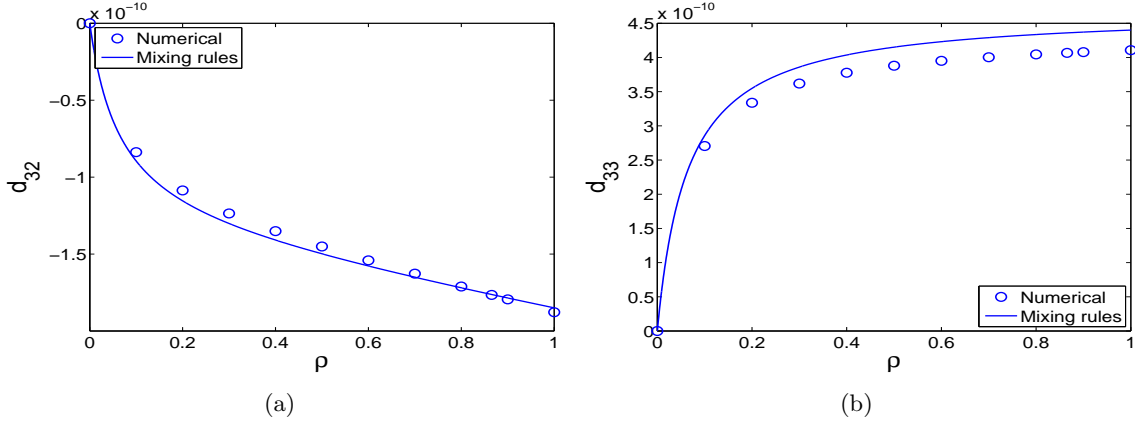
Figure 8: Evolution of piezoelectric properties of d_{33} MFCs as a function of the fiber volume fraction : comparison between the mixing rules and the finite element computations

5 Comparison with experimental results

The mixing rules can be used to compute the equivalent properties of the **active layer** of MFCs. The volume fraction of fibers is approximately 86 % (estimated value from data given by *SmartMaterial*). The calculated homogenized properties for this volume fraction are given in Table 3 for d_{31}-MFCs (material properties considered in section 4 are used), and in Table 4 for d_{33}-MFCs

d_{31} MFC Homogenized Properties	Symbol	Unit	Mixing rules
Young's modulus	E_L	GPa	47.17
	E_T	GPa	16.98
Shear Modulus	G_{LT}	GPa	6.03
	G_{Tz}	GPa	6.06
	G_{Lz}	GPa	17.00
Poisson's ratio	ν_{LT}	-	0.395
Piezoelectric charge constants	d_{31}	pC/N	-183
	d_{32}	pC/N	-153
Dieletric relative constant (free)	$\varepsilon^T_{33}/\varepsilon_0$	-	1600

Table 3: Homogenized properties of the active layer of d_{31}-MFCs calculated using the analytical mixing rules of Table 1

d_{33} MFC Homogenized Properties	Symbol	Unit	Mixing rules
Young's modulus	E_L	GPa	42.18
	E_T	GPa	16.97
Shear Modulus	G_{LT}	GPa	6.03
	G_{Tz}	GPa	17
	G_{Lz}	GPa	6.06
Poisson's ratio	ν_{LT}	-	0.380
Piezoelectric charge constants	d_{32}	pC/N	-176
	d_{33}	pC/N	436
Dieletric relative constant (free)	$\varepsilon_{33}^T/\varepsilon_0$	-	1593

Table 4: Homogenized properties of the active layer of d_{33}-MFCs calculated using the analytical mixing rules of Table 1

Unfortunately, there are no direct measurements of such properties available in the literature or in the datasheet. **Experiments have only been performed on the packaged MFC transducers, and not on the active layer alone**. Experimentally, in-plane mechanical properties and free strains of the MFC have been measured.

5.1 In plane mechanical properties

The in plane mechanical properties of the MFC can be computed using classical laminate theory, if the properties of each layer are known. Figure 9 shows the sequence of layers for a MFC (approximate data provided by the manufacturer *Smart Material* and from [24])
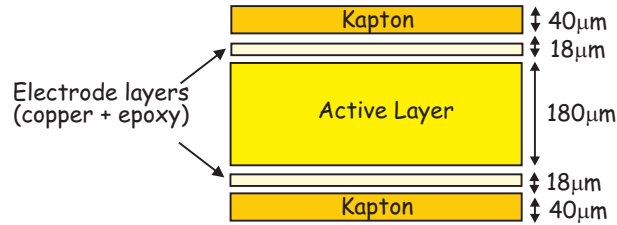

Figure 9: Sequence of layers for the MFC. Approximate data provided by *Smart Material*

For the kapton layers, the following properties are used :

$$1/s_{11}^E = 1/s_{22}^E = 1/s_{33}^E = 2.8 GPa \quad \nu = 0.3$$

For a d_{33}-MFC, the electrode layers are made of an epoxy matrix and copper fibers, oriented perpendicular to the PZT fibers. The volume fraction of copper is approximately 24% and the following properties are used for the copper :

$$1/s_{11}^E = 1/s_{22}^E = 1/s_{33}^E = 117.2 GPa \quad \nu = 0.31$$

The equivalent properties of this layer are computed using the classical mechanical mixing rules. In Table 5, the in-plane mechanical properties of d_{33}-MFCs are computed from the properties of all the layers, and compared with published analytical and experimental values for a 'Reference MFC' manufactured in the early developments of such devices [24], as well as data from the manufacturer. Our values are in good agreement with experimental results, despite the uncertainty on the values of certain material properties and layers thicknesses. Note that there are no experimental or analytical results available for d_{31}-MFCs, but the properties should be similar to d_{33}-MFCs, as can be seen from the values in Table 3.

	Analytical [24]	Experiment [24]	Smart Mat. datasheet	Present study
E_L (GPa)	31.2	29.4	30.34	27.27
E_T (GPa)	17.05	15.2	15.86	14.76
ν_{LT}	0.303	0.312	0.31	0.32
$G_{12}(GPa)$	5.27	6.06	5.52	4.13

Table 5: Comparison of analytical predictions and experimental values of mechanical properties of d_{33}-MFCs

5.2 Free strain measurements

Free strain measurements consist in applying a voltage difference across the electrodes and measuring the elongation of the MFC both in the longitudinal and the transverse directions. The free strain in the fiber direction $\S_L$ is directly related to the applied voltage V and the longitudinal piezoelectric coefficient. One can show that the passive layers, because they are soft compared to the PZT material, have little effect (2 to 3 % difference) on the free strain of the MFC, so that it can be assumed that it is equal to the free strain of the active layer.

For a d_{33}-MFC we have :

$$S_L = d_{33}\frac{V}{p} \tag{28}$$

where p is the distance between two finger electrodes (0.5 mm). For d_{31}-MFCs, the free strain in the longitudinal direction is given by :

$$S_L = d_{31}\frac{V}{h} \tag{29}$$

where h is the thickness of the transducer (0.18 mm). The free strains in the longitudinal direction are computed and compared with the values from the datasheet, given in ppm/V (10^{-6}/Volt) in Table 6. A good agreement is found for both types of MFCs. For d_{33}-MFCs, the d_{32} and d_{33} coefficients have been identified from measurements and are available on the datasheet. These values are compared with the mixing rules result in Table 7. Here again a good agreement is found. Note that such results are not available for d_{31}-MFCs.

d_{31}-MFC analytical	d_{31}-MFC datasheet	d_{33}-MFC analytical	d_{33}-MFC datasheet
1.02 ppm/V	1.1-1.3 ppm/V	0.87 ppm/V	.75-.9 ppm/V

Table 6: Comparison of analytical predictions and experimental values of longitudinal free strains

d_{33} analytical	d_{33} datasheet	d_{32} analytical	d_{32} datasheet
436 pC/N	467 pC/N	-176 pC/N	-199 pC/N

Table 7: Comparison of analytical predictions and experimental values of d_{32} and d_{33} for d_{33}-MFCs

6 Conclusion

Piezocomposite actuators and sensors are used in many active control applications such as active damping or morphing. This paper is focused on Macro Fiber Composites (MFCs) transducers. The modelling of structures equipped with such transducers is problematic because the data sheet from the manufacturer does not contain all the necessary information. In order to overcome this problem, we have investigated the possibility to evaluate equivalent, homogeneous properties from the constituent properties. Simple analytical mixing rules have been derived based on the Uniform Field Method (UFM), using the plane stress hypothesis. In particular, mixing rules for the piezoelectric coefficients of both for d_{31} and d_{33}-MFCs have been presented. These mixing rules have been validated based on 3D piezoelectric finite element computations and experimental results available from the literature or the datasheet of the manufacturer. Such simple rules can also serve as useful guidelines for the engineers in the design of piezocomposite transducers with rectangular fibers for a given application (i.e. directional sensing or actuation).

7 Acknowledgements

References

[1] S. Gebhardt, L. Seffner, F. Schlenkrich, and A. Schonecker. PZT thick films for sensor and actuator applications. *Journal of the European Ceramic Society*, 27:4177–4180, 2007.

[2] A.A. Bent, N.W. Hagood, and J.P. Rodgers. Anisotropic actuation with piezoelectric fiber composites. *J. Intell. Mater. Syst. Struct*, 6:338–349, 1995.

[3] N.W. Hagood, R. Kindel, K. Ghandi, and P. Gaudenzi. Improving transverse actuation of piezoceramics using interdigitated surface electrodes. In N. W. Hagood, editor, *Proc. SPIE Vol. 1917, p. 341-352, Smart Structures and Materials 1993: Smart Structures and Intelligent Systems, Nesbitt W. Hagood; Ed.*, volume 1917, pages 341–352, 1993.

[4] A.A. Bent and N.W. Hagood. Piezoelectric fiber composites with interdigitated electrode. *J. Intell. Mater. Syst. Struct*, 8:903–919, 1997.

[5] W.K. Wilkie et al. Low-cost piezocomposite actuator for structural control applications. In *Proc. SPIE 7th Annual Int. Symp. Smart. Struct. Mater.*, Newport Beach, USA, 2000.

[6] B.R. Williams, G. Park, D.J. Inman, and W.K. Wilkie. An overview of composite actuators with piezoceramic fibers. In *Proc. of 20th Int. Modal Analysis Conference (IMAC)*, Los Angeles, USA, 2002.

[7] P. Wierach. Low profile piezo actuators based on multilayer technology. In *Proc. of 17th Int. Conf. on Adaptive Structures and Technologies (ICAST2006)*, Taipei, Taiwan, October 2006.

[8] Vincent Piefort. *Finite Element Modelling of Piezoelectric Active Structures*. PhD thesis, Université Libre de Bruxelles, June 2001.

[9] U. Gabbert, H. Köppe, F. Seeger, and H. Berger. Modeling of smart composite shell structures. *J. of th. And appl Mechanics*, 3(40):575–593, 2002.

[10] A. A. Bent. Piezoelectric fiber composites for structural actuation. Master's thesis, Massachusetss Institute of Technology, 1994.

[11] A. A. Bent. *Active Fiber Composites for Structural Actuation*. PhD thesis, Massachusetss Institute of Technology, 1997.

[12] D.P. Skinner, R.E. Newnham, and L.E. Cross. Flexible composite transducers. *Mat. Res. Bull.*, 13:599–607, 1978.

[13] R. Hill. A self consistent mechanics of composite materials. *Journal of Mechanics and Physics of Solids*, 13:213–222, 1965.

[14] R.B. Williams, D.J. Inman, and W.K. Wilkie. Temperature-dependent coefficients of thermal expansion in macro fiber composite actuators. In *5th International Congress on Thermal Stresses*, Blacksburg, VA, June 2003.

[15] B.R. Williams, B.W. Grimsley, D.J. Inman, and W.K. Wilkie. Manufacturing and mechanics-based characterization of Macro Fiber Composite actuators. In *Proc. of IMECE'02*, New Orleans, Louisiana, USA, 2002.

[16] R.B. Williams, D.J. Inman, and W.K. Wilkie. Nonlinear mechanical behavior of macro fiber composite actuators. In *6th International Conference on Sandwich Structures*, Ft. Lauderdale, FL, March 2003.

[17] R.B. Williams, M.R. Schultz, M.W. Hyer, D.J. Inman, and W.K. Wilkie. Nonlinear tensile and shear behavior of macro fiber composite actuators. In *The American Society for Composites 18th Technical Conference*, Gainesville, FL, October 2003.

[18] A. Deraemaeker and A. Preumont. Piezoelectric structures : modeling for control. In *Proc. Ninth International Conference on Recent Advances in Structural Dynamics*, Southampton, UK, 2006.

[19] A. Deraemaeker, S. Benelechi, A. Benjeddou, and A. Preumont. Analytical and numerical computation of homogenized properties of MFCs : Application to a composite boom with MFC actuators and sensors. In *Proc. III ECCOMAS thematic conference on Smart Structures and Materials*, Gdansk, Poland, July 2007.

[20] P. Tan and L. Tong. Micro-electromechanics models for piezoelectric-fiber-reinforced composite materials. *Composites Science and Technology*, 61:759–769, 2001.

[21] B. Agarwal and L. Broutman. *Analysis and performance of fiber composites (2nd Edition)*. John Wiley & Sons, 1990.

[22] R.A. Schapery. Thermal expansion coefficients of composite materials based on energy principles. *Journal of Composite Materials*, 2(3):380–404, 1968.

[23] Samcef from samtech, http://www.samtech.be.

[24] R.B. Williams. *Nonlinear mechanical and actuation characterization of piezoceramic fiber composites*. PhD thesis, Blacksburg (VA), USA, 2004.